ACS APPLIED MATERIALS & INTERFACES

www.acsami.org

Research Article

Ultraconformal Skin-Interfaced Sensing Platform for Motion Artifact-Free Monitoring

Yuyan Gao,[§] Bowen Li,[§] Ling Zhang, Xianzhe Zhang, Xin Xin, Senpei Xie, Ryan Allen Lee, Kang Li, Weiwei Zhao, and Huanyu Cheng*

Cite This: *ACS Appl. Mater. Interfaces* 2024, 16, 27952−27960

Read Online

ABSTRACT: Capable of directly capturing various physiological signals from human skin, skin-interfaced bioelectronics has emerged as a promising option for human health monitoring. However, the accuracy and reliability of the measured signals can be greatly affected by body movements or skin deformations (e.g., stretching, wrinkling, and compression). This study presents an ultraconformal, motion artifact-free, and multifunctional skin bioelectronic sensing platform fabricated by a simple and user-friendly laser patterning approach for sensing high-quality human physiological data. The highly conductive membrane based on the room-temperature coalesced Ag/Cu@Cu core−shell nanoparticles in a mixed solution of polymers can partially dissolve and locally deform in the presence of water to form conformal contact with the skin. The resulting sensors to capture improved electrophysiological signals upon various skin deformations and other biophysical signals provide an effective means to monitor health conditions and create human-machine interfaces. The highly conductive and stretchable membrane can also be used as interconnects to connect commercial off-the-shelf chips to allow extended functionalities, and the proof-of-concept demonstration is highlighted in an integrated pulse oximeter. The easy-to-remove feature of the resulting device with water further allows the device to be applied on delicate skin, such as the infant and elderly.

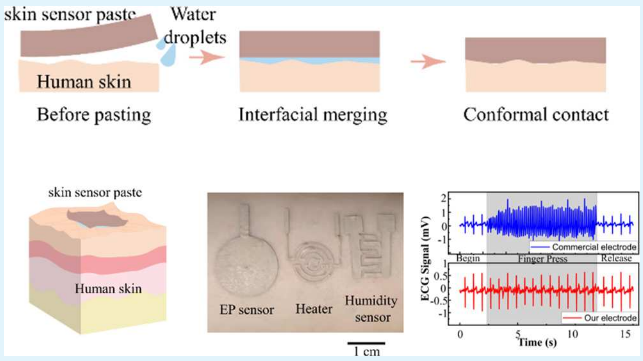

KEYWORDS: *wearable bioelectronics, motion artifact-free, intrinsically conductive and stretchable nanocomposite, room-temperature coalescence, electrophysiological signals, Ag/Cu@Cu core−shell nanoparticles*

1. INTRODUCTION

Skin-interfaced bioelectronics has emerged as a promising technology for health monitoring and disease treatment.[1−4] These device platforms can collect physiological signals and biochemical information for early health diagnosis, as well as provide stimulation for drug delivery and disease treatment.[5−11] However, the accuracy of the obtained signals is often affected by motion artifacts from body movements and natural skin motions (e.g., stretching, compression, and bending). Although postprocessing strategies have been explored to remove noise from the obtained signals, useful information is inadvertently filtered out and the algorithm is not universally applicable.[12−14] Therefore, it is highly desirable to exploit motion artifact-free sensors and devices. As a result, skin-interfaced bioelectronics are designed to be flexible, stretchable, and conformal to the human skin so as to deform with the skin. Advanced materials and design strategies include the use of strain isolation, stretchable conductors, or multiple sensors for postprocessing.[15−17] However, they often need to use high-cost and multistep chemical synthesis, sensor/device-specific designs, or complicated and integrated semiconductor chips. Therefore, it is of high interest to develop a simple, universal, low-cost, and scalable material and sensing platform for motion artifact-free monitoring of various biophysical and biochemical signals.

This study presents a multifunctional device platform based on a simple yet versatile fabrication approach to collect motion artifact-free, high-quality physiological signals. The fabrication relies on the laser patterning of a highly conductive and stretchable thin film that exploits Ag/Cu@Cu nanoparticles coalesced at 50 °C in a mixed solution of montmorillonite (MMT), poly(vinyl alcohol) (PVA) solution, glycerol, and poly(ethylene glycol) (PEG) (Figure S1). Contributed by MMT and PVA, the resulting skin-interfaced flexible and stretchable bioelectronics can partially dissolve by water and moisture and locally deform to form conformal contact with the skin. The montmorillonite-mixed Ag/Cu@Cu thin film is

Received: March 15, 2024
Revised: April 27, 2024
Accepted: May 8, 2024
Published: May 14, 2024

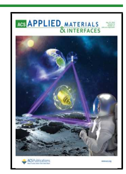

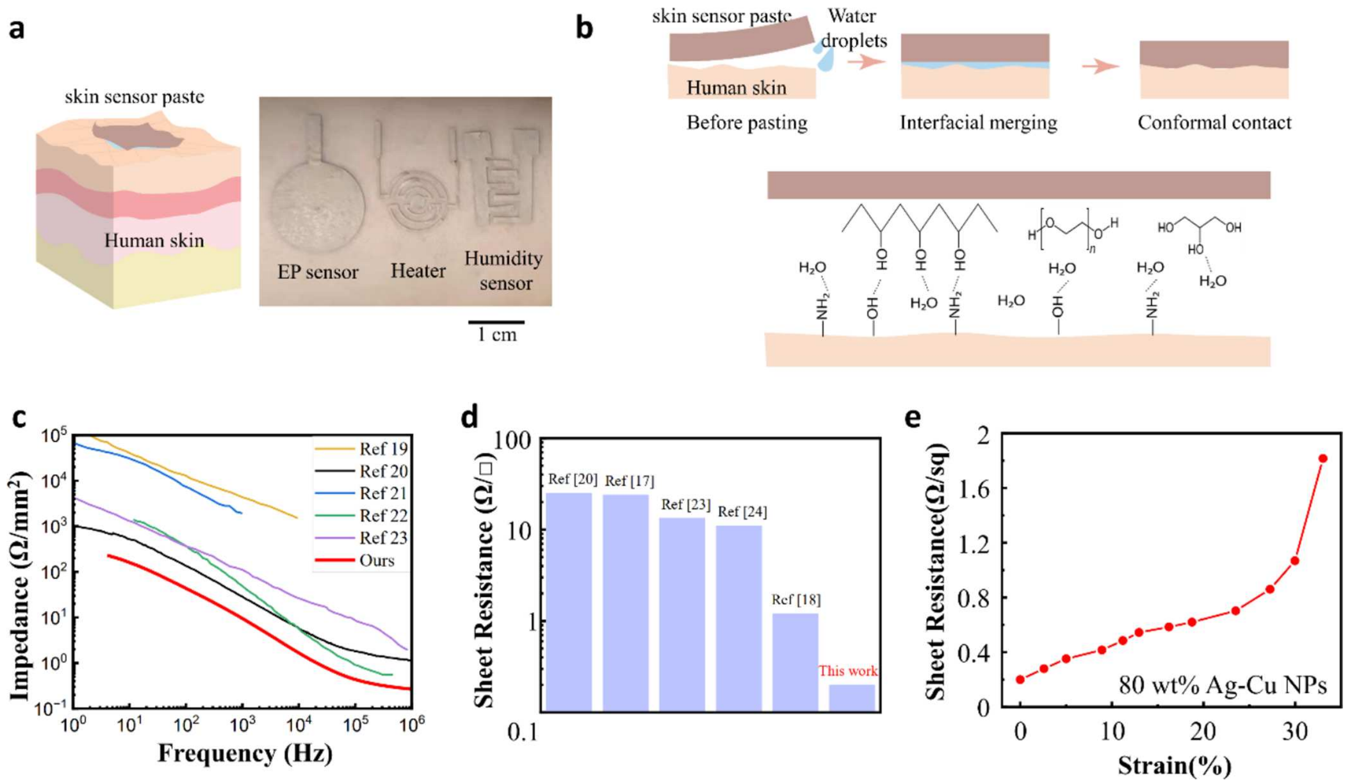

Figure 1. Overview and design of the skin-interfaced, ultraconformal, multifunctional bioelectronics for motion artifact-free monitoring of human physiological signals. (a) Schematic (left) and demonstration (right) of the conformal stretchable multifunctional device platform on a human forearm. (b) Schematic showing the mechanism of the ultraconformal device/skin interface from partial dissolution and local deformation assisted by water molecules. (c) Low contact impedance, (d) low sheet resistance, and (e) high electromechanical performance of the conformal stretchable thin film (80 wt % Ag−Cu NPs).

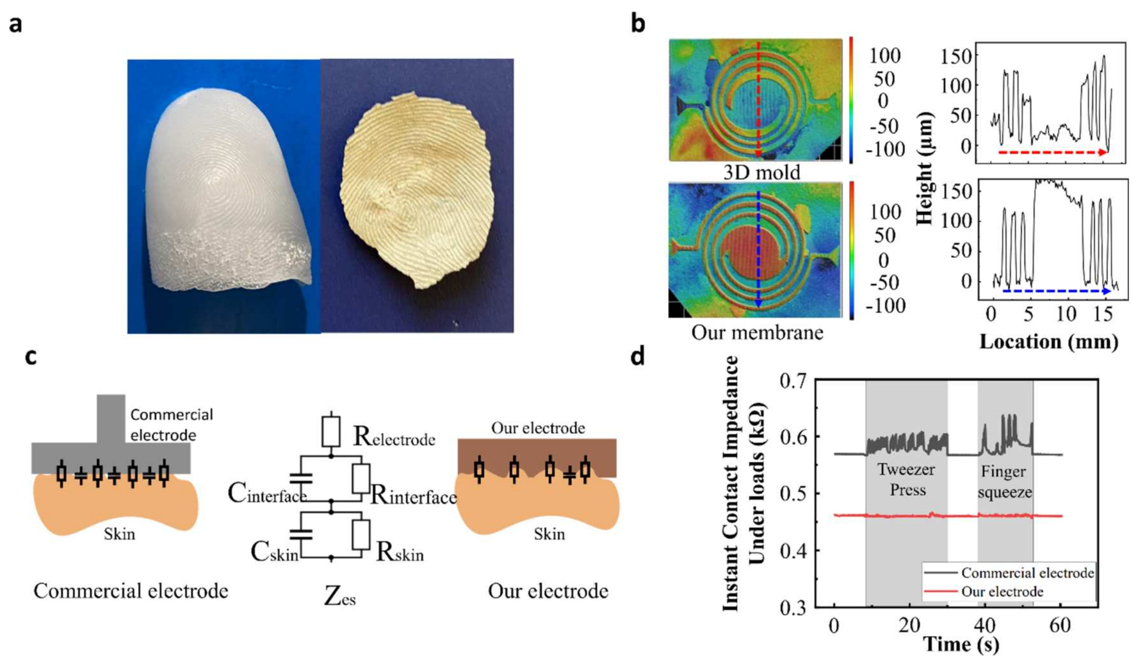

Figure 2. Demonstration of the ultraconformal contact. (a) Photos of a wax-based finger mold and the conformed stretchable thin film with the corresponding fingerprint pattern. (b) Optical profilometer image (left) and comparison analysis (right) of the surface morphology between the two. (c) Schematic showing the modeling of the contact impedance at the electrode-skin interface. (d) Comparison of the contact impedance between the conformal stretchable (red) and commercial get electrodes (black) with and without external perturbations.

unique in the interfacial deformable mechanism to achieve ultraconformal contact with high conductivity and stretchability for artifact-free monitoring of high-quality physiological signals. The demonstrated wearable devices include electrophysiological (EP) sensors for electrocardiography (ECG), electromyography (EMG), and electroencephalography

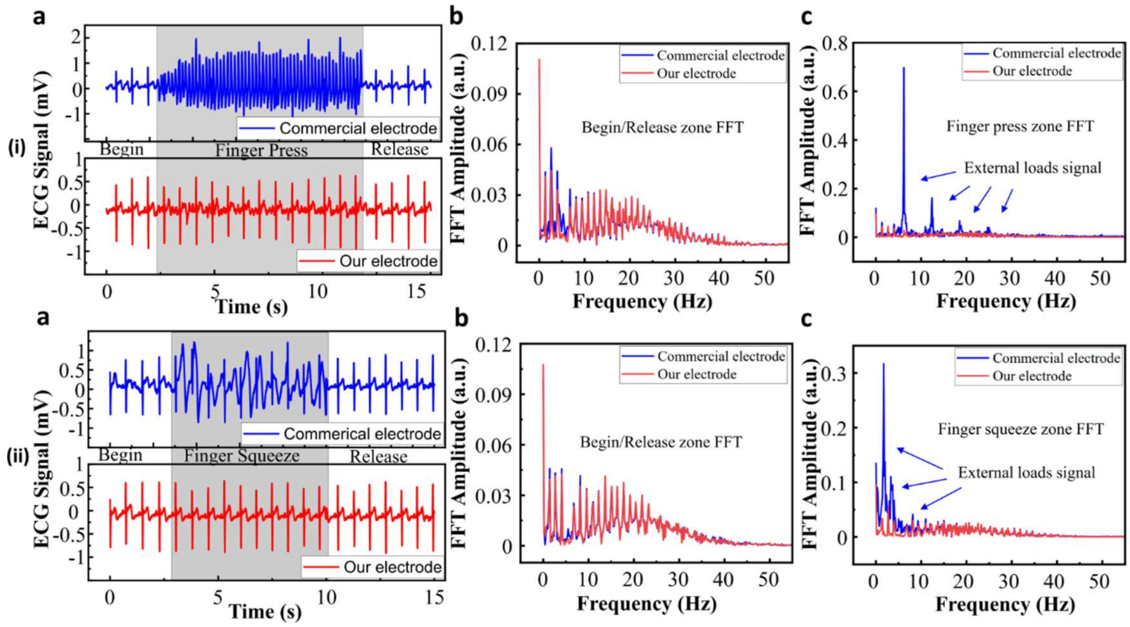

Figure 3. Demonstration and analysis of motion artifact-free electrophysiological sensing. Comparison of ECG signals between conformal stretchable (red) and commercial gel electrodes (blue) in time and frequency domains. ECG signals in (a) the time domain and (b) before and (c) after motions in the frequency domain for (i) finger pressing and (ii) finger squeezing.

(EEG), as well as humidity and temperature sensors. The integration of commercial off-the-shelf (COTS) chips further expanded the device functionalities, and the concept is demonstrated through an integrated oximeter to measure pulse rate and blood oxygen saturation. Besides health monitoring, gesture recognition provided by the detected EMG signals also leads to a human-machine interface. The design strategies and fabrication approaches presented in this study could also be leveraged for other wearable biophysical and biochemical sensors for motion artifact-free sensing.

2. RESULTS

2.1. Material Performance. The nanocomposite thin film features exceptional interfacial conformability, high electrical conductivity, and good stretchability (Figure 1). Facilitated by interlayer water molecules, the thin film forms a conformal contact with the skin (Figure 1a). By exploiting a simple laser patterning process, various high-performance skin-interfaced sensors can be facilely fabricated, including EP, humidity, temperature sensors, and heaters. The excellent interfacial conformability results from partial dissolution and local deformation of the MMT and PVA (Figure 1b). Furthermore, the massive presence of hydroxyl group (−OH) in PVA and glycerol enhances the hydrophilicity to result in strong adhesion to human skin in the presence of water molecules.

The excellent contact at the electrode/skin interface results in low areal contact impedance over a wide range of frequencies (Figure 1c), which is significantly lower than those previously reported based on flexible materials.[18−23] In addition, the thin film exhibits excellent electrical conductivity with reduced sheet resistance compared to the previous reports based on flexible materials (Figure 1d).[17,18,20,23,24] The high conductivity can also be well maintained upon stretching of >30% (Figure 1e), which is larger than the maximum strain on the skin.[25] The outstanding conformal contact, high electrical conductivity, and stretchability are ideal for motion artifact-free sensing and on-skin bioelectronics.

Partial dissolution and local deformation allow the thin film to conform to the skin. The conformal contact is quantified by comparing the 3D morphology of the wax mold of thumbprint patterns and the conformed thin film (Figure 2a). After partial dissolution and local deformation, the thin film conforms to the wax mold with hierarchical fingerprint structures. The morphologies of the 3D wax mold and the conformal thin film captured by the optical profilometer both show distinct peaks and valleys on the surface (Figure 2b). The average heights between peaks and valleys exhibit a high degree of similarity for the 3D max mold (119.79 μm) and thin film (135.13 μm), suggesting an excellent match of 88.65% in the interfacial morphology.

The conformal contact contributes to the measured low contact impedance at the electrode/skin interface. The electrode-skin impedance (Z_{es}) is composed of several components, including the electrode resistance ($R_{electrode}$), the electrode-skin contact resistance ($R_{interface}$), the electrode-air-skin capacitance ($C_{interface}$), and the skin impedance ($R_{skin} \parallel C_{skin}$) (Figure 2c).[26,27] The amplitude of the overall impedance (Z_{total}) between two electrodes is the sum of two electrode-skin impedances ($Z_{es1}$and Z_{es2}) and the bioimpedance of the human body (Z_{bio}): $|Z_{total}| = |Z_{es1} + Z_{es2} + Z_{bio}|$. The highly conductive electrode (and commercial gel electrode) exhibits a small electrode resistance ($R_{electrode}$), which has a negligible effect on the total impedance.With water at the interface, the stratum corneum becomes hydrated to give a lower resistance (R_{skin}). More importantly, the partial dissolution and local deformation of the thin film with the semi-dry electrode allow it to fill the air gap at the electrode/skin interface for decreased electrode-skin capacitance ($C_{interface}$). Taken together with the increased contact area (A) for reduced contact resistance ($R_{interface}$) after local deformation, the overall low impedance at the electrode/skin interface is achieved. The increased size of the electrodes also decreased the contact impedance (Figure S2).

https://doi.org/10.1021/acsami.4c04357
ACS Appl. Mater. Interfaces 2024, 16, 27952−27960

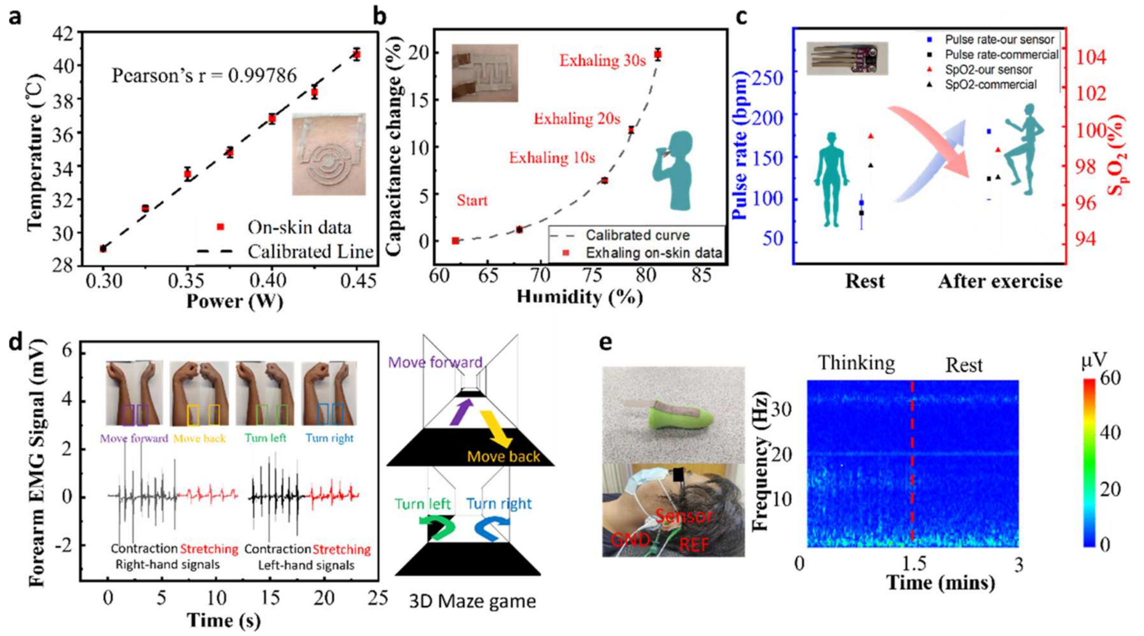

Figure 4. Applications and demonstrations of the conformal multifunctional bioelectronics. (a) Dependence of the output peak temperature of the on-skin spiral-shaped heater on the input power. (b) Capacitance change of the humidity sensor as a function of human hydrous exhaling at different durations. The error bars were based on standard deviation from three measurements. (c) Measured pulse rate (blue) and SpO_2 level (red) from the integrated oximeter at the fingertip before and after the 2 min exercise. (d) Human-machine interface based on the EMG electrodes to control the game character with bimanual gestures. (e) (Left) Experimental setup of and (right) the collected brain wavelength contour from the in-ear EEG sensor consisting of the conformal stretchable patterned thin film on a commercial deformable foam earplug in thinking mode (0−1.5 min) and rest mode (1.5−3 min).

Thanks to the flexible and stretchable properties, the thin film deforms with the skin during various mechanical deformations, leading to minimal changes in the effective contact area and interfacial gap distance. As a result, the low contact impedance can be maintained to ensure a high signal quality and low noise. For instance, the skin-electrode contact impedance at 100k Hz remains at a consistently low value under external interference from tweezer pressing and finger squeezing (Figure 2d). In contrast, the commercial gel electrode shows a large fluctuation in the impedance during external perturbation.

The high conductivity of the thin film can be attributed to the use of highly concentrated conductive Ag/Cu@Cu NPs. As the concentration of Ag/Cu@Cu NPs increases from 60 to 80 wt % with a step size of 5 wt % (i.e., 60, 65, 70, 75, and 80 wt %), the contact of the metal NPs at the micrometer scale also increases as observed in the SEM image (Figure S3). As a result, the sheet resistance is significantly reduced (Figure S4).

2.2. Motion Artifact-Free EP Sensing with Electrodes. The ultraconformality and low contact impedance over deformation allow the resulting electrodes for motion artifact-free sensing of EP signals. As a representative example, the ECG signals collected by the three-lead conformal stretchable electrodes (Figure S5) are not affected by the various external perturbations such as finger pressing and squeezing, whereas those from the commercial gel electrodes show significant fluctuations (Figure 3). The signal-to-noise ratio (SNR) that measures the strength of a signal relative to the background noise is used to evaluate the performance of electrodes in the time domain. The value of SNR can be determined from the following equation: $\mathrm{SNR} = 20\log(V_s/V_n)$, where V_s represents the peak-to-peak amplitude of the signal (the difference between the R and S peaks of the PQRST cycle in the ECG signal) and V_n corresponds to the peak-to-peak amplitude of the noise.[28,29] The SNR of the ECG signals from the conformal stretchable electrodes exhibits only a slight decrease from 20.24 to 17.51 as the finger press is applied (Figure 3i(a)). In comparison, the commercial gel electrodes demonstrate a smaller SNR of 18.02 before the deformation and further fail to capture clear ECG signals under deformation, which is likely attributed to significant deformation near the rigid plastic shell.

Transforming the ECG data from the time to frequency domain using the Fourier transform further reveals the impact of external mechanical deformations on the captured signals. Without external deformation, a high correlation in the Fourier-transformed ECG data between the conformal stretchable and commercial gel electrodes is observed to validate the accuracy of the conformal stretchable electrode (Figure 3i(b)). As the finger pressing is applied, several sharp spikes with a frequency corresponding to the external loads show up in the signals captured by the commercial gel electrodes (Figure 3i(c)). In contrast, no significant changes are observed in the signals captured by the conformal stretchable electrode, indicating motion artifact-free sensing of the EP signals with high accuracy and reliability. The impact of finger squeezing on ECG signals is similar to that of finger pressing in both the time domain and frequency domains (Figure 3ii).

Similarly, the conformal stretchable electrodes can measure EMG signals from curvilinear surfaces such as facial muscles (Figure S6) and finger muscles (Figure S7) even in extension mode (Figure S8), whereas commercial gel electrodes fail to do so. Compared with commercial electrodes, the sensors from this work are less affected (less voltage change) by the deformation from external loads (Figure S9).

https://doi.org/10.1021/acsami.4c04357
ACS Appl. Mater. Interfaces 2024, 16, 27952−27960

Table 1. Performance Comparison between the Heater from This Work and Those from Others in the Literature

heater material	R_s (Ω/sq)	area (cm^2)	temperature (°C)/applied voltage (V)	reference
graphene oxide	1568	2 × 1.4	150/60	[33]
Ag NW	30	1.5 × 1	150/10	[34]
metallic glass	3.8	2 × 2	120/5	[35]
cupronickel	16.2	2.5 × 2.5	135/6	[36]
Ag/graphene	4	5 × 5	135/4	[37]
Ag/Cu/MMT/PEG	0.2	2 × 2	140/1.2	this work

Table 2. Performance Comparison between Capacitive Humidity Sensors

sensitivity	material	humidity range	reference
2.8 pF/%RH	zinc oxide	40−90%RH	[48]
0.85 pF/%RH	PMDA-ODA-TiO_2	10−90%RH	[49]
4 pF/%RH	Al_2O_3	5−85%RH	[50]
8.2 pF/%RH	$CaCl_2$	30−95%RH	[51]
1.8 nF/%RH	PIL	10−80%RH	[52]
1.6 nF/%RH	Zn_2SiO_4	11−95%RH	[53]
1.9 nF/%RH	Ag/Cu/MMT/PEG/glycerol	30−90%RH	this work

2.3. Demonstration and Application of Various On-Skin Bioelectronics. The simple laser patterning approach can also prepare a variety of on-skin sensors with complex geometric patterns such as heaters/temperature sensors, humidity sensors, pulse oximeters, and in-ear EEG sensors for health monitoring as well as a human-machine interface for game control. As flexible resistive heaters based on Joule heating are important for thermotherapy, an on-skin, spiral-shaped heater controlled by the input power is calibrated against a commercial thermometer (Figure S10) and demonstrated for efficient heating (Figure 4a) toward wound healing and thermal management.[30−32] The output peak temperature exhibits a strong linear relationship with the input power, with Pearson's linear correlation coefficient of 0.9979. Compared with previously reported soft heaters (Table 1), our spiral-shaped heater exhibits low sheet resistance, low drive voltage, and high heating temperature.[33−37]

The humidity sensor is also very important to detect changes in moisture levels during respiration and skin perspiration.[38−41] The former can be used to estimate health conditions, whereas the latter allows the characterization of skin conditions and barrier functions.[42−45] Designed in an interdigital electrode (Figure 4b), the on-skin humidity sensor can detect the changes in humidity levels on the skin surface through the measured capacitance. After the calibration with a commercial humidity sensor (Figure S11), humidity changes on the skin surface can be successfully measured during hydrous exhalation for various durations. The sensitivity of the humidity sensor is obtained as the ratio of the measured capacitance difference to the relative humidity difference, i.e., sensitivity = $(C_{final} - C_{ref})/(RH_{final} - RH_{ref})$.[46,47] The sensitivity of 1.913 nF/%RH in the range of 30−90% from our humidity sensor is comparable to the previously reported values (Table 2).[47−52]

The highly conductive property of the conformal stretchable material can be used as interconnects to fabricate the flexible and stretchable printed circuit board. The integration of multifunctional sensors with commercial off-the-shelf chips allows for enhanced data processing/transmission capabilities to provide continuous health monitoring and early diagnosis.[53] In a proof-of-concept demonstration, connecting the MAX 30100 sensing chip with an Arduino UNO microcontroller yields an integrated pulse oximeter (Figure 4c). The measured changes in pulse rate and blood oxygen saturation (SpO2) levels before and after a 2 min exercise agree reasonably well with those obtained from the commercial Fingertip Pulse Oximeter (Santa Medical).

By facilitating efficient and effective communication between humans and machines, the human-machine interface combined with artificial intelligence can provide intuitive and user-friendly means to help humans interact with and manage complex systems.[54,55] As a first step toward such a target, the acquired EMG signals from the inner side of both forearms are used to control a 3D maze game programmed in MATLAB in real time (Figure 4d). By bending the wrist inward or outward (muscle contraction or stretching), distinct peak amplitudes in the EMG signals generate four gestures or commands to control the virtual person for moving forward, back, left, and right in the 3D maze game. With each gesture repeated 110 times, the demonstration achieves a high accuracy of more than 95.5% in gesture recognition with the human-machine interface (Table S1), demonstrating high robustness and reliability. Further demonstrations of gesture recognition include eye movements (Figure S12) and hand gestures (Figure S13).

An accurate sleep study for cognitive evaluation relies on the measurement of EEG signals for an extended duration. Further analysis of sleep EEG signals can help reveal sleep patterns and brain activities, such as identifying biomarkers in depression, tracking rapid eye movement, and understanding anesthetic sedation.[56−58] An in-ear EEG sensor that combines stretchable electrodes with commercial deformable foam earplugs is further designed to reduce interference during sleep (Figure 4e). The feasibility of the in-ear EEG sensor is first confirmed in a short-period EEG measurement during the thinking period (0−1.5 min) and resting period (1.5−3 min). The EEG frequency contour shows an obvious β brain wave at 10−20 Hz only during the thinking period (Figure 4e). As a brain activity signature for alertness, concentration, and thinking, the β wave in the EEG frequency contour collected by our electrodes differentiates thinking from resting. The EEG signals collected from various shapes of earplugs are relatively robust for different individuals (Figure S14). To further improve spatial resolution and reduce the blurring effect due to volume conduction from multiple electrodes, tripolar EEG

https://doi.org/10.1021/acsami.4c04357
ACS Appl. Mater. Interfaces 2024, 16, 27952−27960

Table 3. Performance Comparison between the Sensor from This Work and Others in the Literature to Detect Electrophysiological Signals

signals	materials	key features	limitations	reference
ECG	polymer, Ag NWs	stretchable, stable	requires tapes for fixing	60
ECG	laser-induced graphene	fast fabrication	high signal-to-noise ratio	61
ECG/EMG	Cu−PI−Au-PDMS	low cost and scalable	weak interfacial adhesion	62
ECG/EMG	PDMS, PEDOT:PSS	breathable, long-term	high cost of materials	63
ECG/EMG/EEG	graphene, PEDOT:PSS	conformal, ultrathin	high cost of materials	17
ECG/EMG	Ag, PEDOT:PSS	conformal, drawn-on-skin	high cost of materials	18
ECG/EMG/EEG	montmorillonite, PVA, Ag/Cu@Cu NPs	artifact-free, conformal, multifunctional	one-time use	this work

electrodes are designed and facilely fabricated by laser patterning to obtain the Laplacian signal (Figure S15). As the second spatial derivative of the collected potentials, surface Laplacian EEG obtained from central and surrounding electrodes is reference-electrode-independent and reduces common noise, providing increased spatial selectivity and decreased mutual information in the measured EEG.[59] The comparison in electrophysiological signals between the sensors from this work and others in the literature indicates very good performance of the artifact-free, ultraconformal, and multifunctional platform (Table 3).[17,18,60−63]

3. CONCLUSIONS

In summary, this work presents a class of conformal stretchable skin bioelectronics based on low-cost and facile laser patterning of a nanocomposite thin film for motion artifact-free sensing of electrophysiological and other biophysical signals. The nanocomposite thin film can be triggered by water molecules to result in partial dissolution and local deformation at the sensor/skin interface. Combined with the highly conductive and stretchable properties, the resulting on-skin electrophysiology (EP) sensors exhibit reduced contact impedance and high signal quality even during mechanical deformations such as compression or stretching. The EP signals collected from this conformal device as a human-machine interface can be used for gesture recognition and game control. Used as stretchable and conductive interconnects, the patterned conformal thin film can facilely integrate with the other commercial COTS chips for extended sensing and processing capabilities. The material can also be easily removed after use (Figure S16 and Supporting Movie 1). The concept is showcased in an integrated oximeter to measure the pulse rate and blood oxygen saturation. The design concepts and application demonstrations of the multifunctional conformal device platform can also be adapted for other biophysical and biochemical sensors for motion artifact-free monitoring for the practical use of next-generation wearable electronics. While the current sensor materials are disposable after use, it would be of high interest to exploit the possibility to potentially recycle and reuse these materials in future studies for sustainable applications.

4. EXPERIMENTAL SECTION

4.1. Materials. Poly(vinyl alcohol) (PVA-124) was purchased from Innochem (Beijing, China). Poly(ethylene glycerol) and montmorillonite (K-10) were obtained from Aladdin (Shanghai, China). Glycerol was purchased from Sinopharm Chemical Reagent Co. (Shanghai, China). The defoamer (BYK-024) was acquired from BYK (Wesel, Germany). Ag−Cu nanoparticles were obtained from Ha Shen Technology (Shenzhen, China).

4.2. Fabrication of the Skin-Conformal Membrane. The fabrication of the skin-conformal membrane started with mixing 9 wt % PVA, 5 wt % PEG, and 4 wt % glycerol in 81 wt % water followed by heating at 90 °C. After adding 1 wt % ST 2436 defoamer to eliminate bubbles, 13 wt % montmorillonite and 66 wt % Ag−Cu NPs were introduced to the 21 wt % obtained solution. Next, the mixture was deposited on a glass slide with a doctor's blade to achieve a uniform membrane. Finally, the membrane was heated to 50 °C for 0.5 h to achieve enhanced electrical conductivity.

4.3. Tensile Test of the Membrane. The membrane was first attached to a soft 00−30 EcoflexTM substrate with a size of 2 cm × 2 cm × 5 mm and then a small amount of water was applied at the interface to improve the adhesion. After clamping both ends of the composite membrane, a custom-built stretcher was used to apply uniaxial tensile strain, and the electrical resistance was simultaneously measured with the Keithley 2401 digital multimeter (Figure S17).

4.4. Fabrication and Characterizations of the Sensors. The different types of sensors with various 2D patterns were designed by AutoCAD and patterned with a CO_2 laser-cutting machine (Universal Laser System, ULS 2.3). The patterned sensors were connected to conductive copper/polyimide (DuPont Pyralux AC Single-side Clad, Copper/Dielectric thickness: 09 μm/12 μm) thin stripes via conductive silver paste (MG Chemicals, 8331D). The electrical resistance of the sensors was measured by connecting the copper stripes to a Keithley 2401 digital multimeter (with data acquisition I−V software) with alligator clips. The sheet resistance R_s was then calculated from the electrical resistance R as $R_s = R{\cdot}L/W$, where L and W are the lengths and widths of the samples. The capacitance of the humidity sensor was measured by an LCR meter (Hioki IM 3536 01). After inserting the arm with the humidity sensor into a sealed jar together with a cup of water, the moisture level from the evaporation of the water in the jar was measured by the changes in the capacitance of the humidity sensor. The power of the heater was provided by a DC power supply (EVENTEK, KPS3010d), and the temperature was captured by the FLIR infrared camera. The impedance was measured by KEYSIGHT E4980A. Electrophysiological signals (e.g., ECG, EMG, and EEG) were collected by Power Lab with Bio Amp (ADInstruments). Fourier transform was obtained by MATLAB using the FFT function. All experiments on human subjects were approved by the Institutional Review Board (IRB) at the Pennsylvania State University (STUDY00008003).

4.5. Measurement and Comparison of Surface Morphology. A PDMS elastomer finger mold was first prepared by curing the precursor (SYLGARD 184, 10:1 ratio, Dow Corning) against the thumb finger. Casting the liquid wax into a PDMS finger mold prepared the wax-based finger mold. Pressing the membrane against the wax-based finger mold for 10 s created the fingerprint on the thin film. The flat PMDS (SYLGARD 184, 10:1 ratio, Dow Corning) substrate with the spiral pattern designed by AutoCAD was created by the CO2 laser system (Universal laser system VLS2.30) with specified parameters (power 10.5%, speed 10 mm/s, PPI 1000). After finger pressing the membrane against the patterned PDMS substrate for 10 s, drying the membrane in the ambient environment was followed by removal from the PDMS surface. The surface morphologies of the dried membrane and patterned PDMS substrate were then measured with an optical profilometry device (Zygo NexView3D).

4.6. Three-Lead ECG Measurement. ECG signals were collected from three-lead electrodes using a Power Lab with Bio Amps from ADInstruments (Figure S18). After placing the electrodes

https://doi.org/10.1021/acsami.4c04357
ACS Appl. Mater. Interfaces 2024, 16, 27952−27960

on the right arm (RA), left arm (LA), and left leg (LL) of the human subject, the electrodes were connected to the common, positive, and negative electrode portals of the Bio Amps. The signals generated by the activities of the cardiac muscles in the cardiovascular cycles were recorded by the computer connected to the Power Lab.

4.7. Tripolar Electrodes for EEG Measurement. After the fabricated electrodes were placed on the scalp, around the ears, and inside of the ear (through earplug insertion) of a human subject, the electrodes connected to the Bio Amps captured the potentials generated from the spontaneous electrical activities of the brain. Next, the Laplacian of the potential ΔP from the tripolar concentric ring electrode was approximately calculated as $\Delta P \cong 16(V_m - V_c) - (V_o - V_c)$, where V_c, V_m, and V_o are the potentials on the center, middle, and outer rings, respectively.[59,64]

4.8. EMG Measurement. After placing the two fabricated electrodes with a reasonable distance on the same muscle of the human subject, connection to the positive and negative electrode portals of Bio Amps enabled detection of the potential generated from the contraction of the muscle.

4.9. Human-Machine Interface Device Setup. EMG signals measured by the Power Lab were transferred to MATLAB for real-time game control. The combined EMG signals obtained from the left and right inner forearm muscles were used to generate four control commands: the extension of the left (or right) forearm with contraction of the right (or left) forearm for "left turn" (or "right turn"), the extension of both for "move forward", and the contraction of both for "move backward". The Support Vector Machine (SVM) algorithm was then used to process the EMG signal peak magnitude for command classification with an accuracy of 95.5%.

ASSOCIATED CONTENT

Data Availability Statement

All data that support this study are available within the article and its Supporting Information. Other relevant data are available from the corresponding authors upon request.

Supporting Information

The Supporting Information is available free of charge at https://pubs.acs.org/doi/10.1021/acsami.4c04357.

Details of fabrication, contact impedance versus frequency, SEM images, sheet resistance versus concentration, three-lead measurements, facial EMG, finger EMG, deformation on physiological signal detection, heater test, humidity test, EOG, resistance change from skin deformation, EEG signals, removal process, tensile test, physiological signal testing setup, accuracy table for gesture recognition, and measurement details of different physiological signals (PDF)

Removal of conformal thin film after use (Movie 1) (MP4)

AUTHOR INFORMATION

Corresponding Author

Huanyu Cheng − *Department of Engineering Science and Mechanics, The Pennsylvania State University, University Park, Pennsylvania 16802, United States;* orcid.org/0000-0001-6075-4208; Email: Huanyu.Cheng@psu.edu

Authors

Yuyan Gao − *Department of Engineering Science and Mechanics, The Pennsylvania State University, University Park, Pennsylvania 16802, United States;* orcid.org/0000-0002-8955-627X

Bowen Li − *Department of Engineering Science and Mechanics, The Pennsylvania State University, University Park, Pennsylvania 16802, United States*

Ling Zhang − *Department of Engineering Science and Mechanics, The Pennsylvania State University, University Park, Pennsylvania 16802, United States; Shenzhen Key Laboratory of Flexible Printed Electronics Technology, School of Materials Science and Engineering, Harbin Institute of Technology (Shenzhen), Shenzhen 518055 Guangdong, China*

Xianzhe Zhang − *Department of Engineering Science and Mechanics, The Pennsylvania State University, University Park, Pennsylvania 16802, United States*

Xin Xin − *Department of Engineering Science and Mechanics, The Pennsylvania State University, University Park, Pennsylvania 16802, United States*

Senpei Xie − *Shenzhen Key Laboratory of Flexible Printed Electronics Technology, School of Materials Science and Engineering, Harbin Institute of Technology (Shenzhen), Shenzhen 518055 Guangdong, China*

Ryan Allen Lee − *Department of Engineering Science and Mechanics, The Pennsylvania State University, University Park, Pennsylvania 16802, United States*

Kang Li − *Shenzhen Key Laboratory of Flexible Printed Electronics Technology, School of Materials Science and Engineering, Harbin Institute of Technology (Shenzhen), Shenzhen 518055 Guangdong, China;* orcid.org/0000-0003-4600-2186

Weiwei Zhao − *Shenzhen Key Laboratory of Flexible Printed Electronics Technology, School of Materials Science and Engineering, Harbin Institute of Technology (Shenzhen), Shenzhen 518055 Guangdong, China;* orcid.org/0000-0002-0373-1146

Complete contact information is available at: https://pubs.acs.org/10.1021/acsami.4c04357

Author Contributions

[§]Y.G. and B.L. contributed equally to this work.

Notes

The authors declare no competing financial interest.

ACKNOWLEDGMENTS

H.C. acknowledges the support provided by NIH (Award Nos. R21EB030140, U01DA056242, and R21OH012220), NSF (grant nos. 2309323, 2319139, and 2243979), and Penn State University.

REFERENCES

(1) Wang, C.; Yokota, T.; Someya, T. Natural biopolymer-based biocompatible conductors for stretchable bioelectronics. *Chem. Rev.* **2021**, *121* (4), 2109−2146.

(2) Chen, X.; Villa, N. S.; Zhuang, Y.; Chen, L.; Wang, T.; Li, Z.; Kong, T. Stretchable supercapacitors as emergent energy storage units for health monitoring bioelectronics. *Adv. Energy Mater.* **2020**, *10* (4), No. 1902769.

(3) Yao, G.; Yin, C.; Wang, Q.; Zhang, T.; Chen, S.; Lu, C.; Zhao, K.; Xu, W.; Pan, T.; Gao, M. Flexible bioelectronics for physiological signals sensing and disease treatment. *J. Materiomics* **2020**, *6* (2), 397−413.

(4) Chen, Y.; Zhang, Y.; Liang, Z.; Cao, Y.; Han, Z.; Feng, X. Flexible inorganic bioelectronics. *npj Flexible Electronics* **2020**, *4* (1), No. 2.

(5) Wu, H.; Gao, W.; Yin, Z. Materials, devices and systems of soft bioelectronics for precision therapy. *Adv. Healthcare Mater.* **2017**, *6* (10), No. 1700017.

(6) Pang, Y.; Yang, Z.; Yang, Y.; Ren, T. L. Wearable electronics based on 2D materials for human physiological information detection. *Small* **2020**, *16* (15), No. 1901124.

(7) Gu, Y.; Zhang, T.; Chen, H.; Wang, F.; Pu, Y.; Gao, C.; Li, S. Mini review on flexible and wearable electronics for monitoring human health information. *Nanoscale Res. Lett.* **2019**, *14* (1), No. 263.

(8) Yu, Y.; Nyein, H. Y. Y.; Gao, W.; Javey, A. Flexible electrochemical bioelectronics: the rise of in situ bioanalysis. *Adv. Mater.* **2020**, *32* (15), No. 1902083.

(9) Yuk, H.; Lu, B.; Zhao, X. Hydrogel bioelectronics. *Chem. Soc. Rev.* **2019**, *48* (6), 1642−1667.

(10) Goncalves, S.; Ribeiro, J.; Silva, A.; Costa, R.; Correia, J. Design and manufacturing challenges of optogenetic neural interfaces: a review. *J. Neural Eng.* **2017**, *14* (4), No. 041001.

(11) Luan, H.; Zhang, Y. Programmable stimulation and actuation in flexible and stretchable electronics. *Adv. Intell. Syst.* **2021**, *3* (6), No. 2000228.

(12) Wasimuddin, M.; Elleithy, K.; Abuzneid, A.-S.; Faezipour, M.; Abuzaghleh, O. Stages-based ECG signal analysis from traditional signal processing to machine learning approaches: A survey. *IEEE Access* **2020**, *8*, 177782−177803.

(13) Nagendra, H.; Mukherjee, S.; Kumar, V. Application of wavelet techniques in ECG signal processing: an overview. *Int. J. Eng. Sci. Res. Technol.* **2011**, *3* (10), 7432−7443.

(14) Satija, U.; Ramkumar, B.; Manikandan, M. S. A review of signal processing techniques for electrocardiogram signal quality assessment. *IEEE Rev. Biomed. Eng.* **2018**, *11*, 36−52.

(15) Jeong, H.; Lee, J. Y.; Lee, K.; Kang, Y. J.; Kim, J.-T.; Avila, R.; Tzavelis, A.; Kim, J.; Ryu, H.; Kwak, S. S. Differential cardiopulmonary monitoring system for artifact-canceled physiological tracking of athletes, workers, and COVID-19 patients. *Sci. Adv.* **2021**, *7* (20), No. eabg3092.

(16) Rodeheaver, N.; Herbert, R.; Kim, Y. S.; Mahmood, M.; Kim, H.; Jeong, J. W.; Yeo, W. H. Strain-Isolating Materials and Interfacial Physics for Soft Wearable Bioelectronics and Wireless, Motion Artifact-Controlled Health Monitoring. *Adv. Funct. Mater.* **2021**, *31* (36), No. 2104070.

(17) Zhao, Y.; Zhang, S.; Yu, T.; Zhang, Y.; Ye, G.; Cui, H.; He, C.; Jiang, W.; Zhai, Y.; Lu, C. Ultra-conformal skin electrodes with synergistically enhanced conductivity for long-time and low-motion artifact epidermal electrophysiology. *Nat. Commun.* **2021**, *12* (1), No. 4880.

(18) Ershad, F.; Thukral, A.; Yue, J.; Comeaux, P.; Lu, Y.; Shim, H.; Sim, K.; Kim, N.-I.; Rao, Z.; Guevara, R. Ultra-conformal drawn-on-skin electronics for multifunctional motion artifact-free sensing and point-of-care treatment. *Nat. Commun.* **2020**, *11* (1), No. 3823.

(19) Takeshita, T.; Yoshida, M.; Takei, Y.; Ouchi, A.; Hinoki, A.; Uchida, H.; Kobayashi, T. Relationship between contact pressure and motion artifacts in ECG measurement with electrostatic flocked electrodes fabricated on textile. *Sci. Rep.* **2019**, *9* (1), No. 5897.

(20) Du, X.; Niu, Z.; Li, R.; Yang, H.; Hu, W. Highly adhesive, washable and stretchable on-skin electrodes based on polydopamine and silk fibroin for ambulatory electrocardiography sensing. *J. Mater. Chem. C* **2020**, *8* (35), 12257−12264.

(21) Baek, J.-Y.; An, J.-H.; Choi, J.-M.; Park, K.-S.; Lee, S.-H. Flexible polymeric dry electrodes for the long-term monitoring of ECG. *Sens. Actuators, A* **2008**, *143* (2), 423−429.

(22) Chlaihawi, A. A.; Narakathu, B. B.; Emamian, S.; Bazuin, B. J.; Atashbar, M. Z. Development of printed and flexible dry ECG electrodes. *Sens. Biosens. Res.* **2018**, *20*, 9−15.

(23) Ji, S.; Wan, C.; Wang, T.; Li, Q.; Chen, G.; Wang, J.; Liu, Z.; Yang, H.; Liu, X.; Chen, X. Water-resistant conformal hybrid electrodes for aquatic endurable electrocardiographic monitoring. *Adv. Mater.* **2020**, *32* (26), No. 2001496.

(24) Sun, B.; McCay, R. N.; Goswami, S.; Xu, Y.; Zhang, C.; Ling, Y.; Lin, J.; Yan, Z. Gas-permeable, multifunctional on-skin electronics based on laser-induced porous graphene and sugar-templated elastomer sponges. *Adv. Mater.* **2018**, *30* (50), No. 1804327.

(25) Maiti, R.; Gerhardt, L.-C.; Lee, Z. S.; Byers, R. A.; Woods, D.; Sanz-Herrera, J. A.; Franklin, S. E.; Lewis, R.; Matcher, S. J.; Carré, M. In vivo measurement of skin surface strain and sub-surface layer deformation induced by natural tissue stretching. *J. Mech. Behav. Biomed. Mater.* **2016**, *62*, 556−569.

(26) Kusche, R.; Kaufmann, S.; Ryschka, M. Dry electrodes for bioimpedance measurements—Design, characterization and comparison. *Biomed. Phys. Eng. Express* **2018**, *5* (1), No. 015001.

(27) Chi, Y. M.; Jung, T.-P.; Cauwenberghs, G. Dry-contact and noncontact biopotential electrodes: Methodological review. *IEEE Rev. Biomed. Eng.* **2010**, *3*, 106−119.

(28) Pei, W.; Zhang, H.; Wang, Y.; Guo, X.; Xing, X.; Huang, Y.; Xie, Y.; Yang, X.; Chen, H. Skin-potential variation insensitive dry electrodes for ECG recording. *IEEE Trans. Biomed. Eng.* **2017**, *64* (2), 463−470.

(29) Yi, N.; Gao, Y.; Verso, A. L., Jr.; Zhu, J.; Erdely, D.; Xue, C.; Lavelle, R.; Cheng, H. Fabricating functional circuits on 3D freeform surfaces via intense pulsed light-induced zinc mass transfer. *Mater. Today* **2021**, *50*, 24−34.

(30) Choi, S.; Park, J.; Hyun, W.; Kim, J.; Kim, J.; Lee, Y. B.; Song, C.; Hwang, H. J.; Kim, J. H.; Hyeon, T. Stretchable heater using ligand-exchanged silver nanowire nanocomposite for wearable articular thermotherapy. *ACS Nano* **2015**, *9* (6), 6626−6633.

(31) Liu, Q.; Tian, B.; Liang, J.; Wu, W. Recent advances in printed flexible heaters for portable and wearable thermal management. *Mater. Horiz.* **2021**, *8* (6), 1634−1656.

(32) Tang, N.; Zheng, Y.; Cui, D.; Haick, H. Multifunctional dressing for wound diagnosis and rehabilitation. *Adv. Healthcare Mater.* **2021**, *10* (22), No. 2101292.

(33) Sui, D.; Huang, Y.; Huang, L.; Liang, J.; Ma, Y.; Chen, Y. Flexible and transparent electrothermal film heaters based on graphene materials. *Small* **2011**, *7* (22), 3186−3192.

(34) Hong, S.; Lee, H.; Lee, J.; Kwon, J.; Han, S.; Suh, Y. D.; Cho, H.; Shin, J.; Yeo, J.; Ko, S. H. Highly stretchable and transparent metal nanowire heater for wearable electronics applications. *Adv. Mater.* **2015**, *27* (32), 4744−4751.

(35) An, B. W.; Gwak, E.-J.; Kim, K.; Kim, Y.-C.; Jang, J.; Kim, J.-Y.; Park, J.-U. Stretchable, transparent electrodes as wearable heaters using nanotrough networks of metallic glasses with superior mechanical properties and thermal stability. *Nano Lett.* **2016**, *16* (1), 471−478.

(36) Kim, H.-J.; Kim, Y.; Jeong, J.-H.; Choi, J.-H.; Lee, J.; Choi, D.-G. A cupronickel-based micromesh film for use as a high-performance and low-voltage transparent heater. *J. Mater. Chem. A* **2015**, *3* (32), 16621−16626.

(37) Kang, J.; Jang, Y.; Kim, Y.; Cho, S.-H.; Suhr, J.; Hong, B. H.; Choi, J.-B.; Byun, D. An Ag-grid/graphene hybrid structure for large-scale, transparent, flexible heaters. *Nanoscale* **2015**, *7* (15), 6567−6573.

(38) Wang, W.; Nayeem, M. O. G.; Wang, H.; Wang, C.; Kim, J. J.; Wang, B.; Lee, S.; Yokota, T.; Someya, T. Gas-Permeable Highly Sensitive Nanomesh Humidity Sensor for Continuous Measurement of Skin Humidity. *Adv. Mater. Technol.* **2022**, *7* (12), No. 2200479.

(39) Yang, L.; Wang, H.; Abdullah, A. M.; Meng, C.; Chen, X.; Feng, A.; Cheng, H. Direct Laser Writing of the Porous Graphene Foam for Multiplexed Electrochemical Sweat Sensors. *ACS Appl. Mater. Interfaces* **2023**, *15* (29), 34332−34342.

(40) Li, B.; Xiao, G.; Liu, F.; Qiao, Y.; Li, C. M.; Lu, Z. A flexible humidity sensor based on silk fabrics for human respiration monitoring. *J. Mater. Chem. C* **2018**, *6* (16), 4549−4554.

(41) Kano, S.; Kim, K.; Fujii, M. Fast-response and flexible nanocrystal-based humidity sensor for monitoring human respiration and water evaporation on skin. *ACS Sens.* **2017**, *2* (6), 828−833.

(42) Lawson, B.; Aguir, K.; Fiorido, T.; Martini-Laithier, V.; Bouchakour, R.; Burtey, S.; Reynard-Carette, C.; Bendahan, M. Skin alcohol perspiration measurements using MOX sensors. *Sens. Actuators, B* **2019**, *280*, 306−312.

(43) Liu, Y.; Li, X.; Yang, H.; Zhang, P.; Wang, P.; Sun, Y.; Yang, F.; Liu, W.; Li, Y.; Tian, Y. Skin-Interfaced Superhydrophobic Insensible

https://doi.org/10.1021/acsami.4c04357
ACS Appl. Mater. Interfaces 2024, 16, 27952−27960

Sweat Sensors for Evaluating Body Thermoregulation and Skin Barrier Functions. *ACS Nano* **2023**, *17* (6), 5588−5599.

(44) Cretikos, M. A.; Bellomo, R.; Hillman, K.; Chen, J.; Finfer, S.; Flabouris, A. Respiratory rate: the neglected vital sign. *Med. J. Aust.* **2008**, *188* (11), 657−659.

(45) Vanegas, E.; Igual, R.; Plaza, I. Sensing systems for respiration monitoring: A technical systematic review. *Sensors* **2020**, *20* (18), 5446.

(46) Vasiljević, D. Z.; Mansouri, A.; Anzi, L.; Sordan, R.; Stojanović, G. M. Performance analysis of flexible ink-jet printed humidity sensors based on graphene oxide. *IEEE Sensors Journal* **2018**, *18* (11), 4378−4383.

(47) Park, S.-J.; Jeon, J.-Y.; Ha, T.-J. Wearable humidity sensors based on bar-printed poly (ionic liquid) for real-time humidity monitoring systems. *Sens. Actuators, B* **2022**, *354*, No. 131248.

(48) Yang, M.-Z.; Dai, C.-L.; Wu, C.-C. Sol-gel zinc oxide humidity sensors integrated with a ring oscillator circuit on-a-chip. *Sensors* **2014**, *14* (11), 20360−20371.

(49) Liu, M.-Q.; Wang, C.; Kim, N.-Y. High-sensitivity and low-hysteresis porous MIM-type capacitive humidity sensor using functional polymer mixed with TiO2 microparticles. *Sensors* **2017**, *17* (2), No. 284.

(50) Islam, T.; Mahboob, M. R.; Khan, S. A. A simple MOX vapor sensor on polyimide substrate for measuring humidity in ppm level. *IEEE Sens. J.* **2015**, *15* (5), 3004−3013.

(51) Komazaki, Y.; Uemura, S. Stretchable, printable, and tunable PDMS-CaCl2 microcomposite for capacitive humidity sensors on textiles. *Sens. Actuators, B* **2019**, *297*, No. 126711.

(52) Wang, W. C.; Tian, Y. T.; Li, K.; Lu, E. Y.; Gong, D. S.; Li, X. J. Capacitive humidity-sensing properties of Zn2SiO4 film grown on silicon nanoporous pillar array. *Appl. Surf. Sci.* **2013**, *273*, 372−376.

(53) Zhang, L.; Ji, H.; Huang, H.; Yi, N.; Shi, X.; Xie, S.; Li, Y.; Ye, Z.; Feng, P.; Lin, T. Wearable circuits sintered at room temperature directly on the skin surface for health monitoring. *ACS Appl. Mater. Interfaces* **2020**, *12* (40), 45504−45515.

(54) Lim, S.; Son, D.; Kim, J.; Lee, Y. B.; Song, J. K.; Choi, S.; Lee, D. J.; Kim, J. H.; Lee, M.; Hyeon, T. Transparent and stretchable interactive human machine interface based on patterned graphene heterostructures. *Adv. Funct. Mater.* **2015**, *25* (3), 375−383.

(55) Zhu, M.; Sun, Z.; Zhang, Z.; Shi, Q.; He, T.; Liu, H.; Chen, T.; Lee, C. Haptic-feedback smart glove as a creative human-machine interface (HMI) for virtual/augmented reality applications. *Sci. Adv.* **2020**, *6* (19), No. eaaz8693.

(56) Murphy, M.; Bruno, M.-A.; Riedner, B. A.; Boveroux, P.; Noirhomme, Q.; Landsness, E. C.; Brichant, J.-F.; Phillips, C.; Massimini, M.; Laureys, S. Propofol anesthesia and sleep: a high-density EEG study. *Sleep* **2011**, *34* (3), 283−291.

(57) Steiger, A.; Kimura, M. Wake and sleep EEG provide biomarkers in depression. *J. Psychiatr. Res.* **2010**, *44* (4), 242−252.

(58) Campbell, I. G. EEG recording and analysis for sleep research. *Curr. Protoc. Neurosci.* **2009**, *49* (1), 10.12. 11−10.12. 19.

(59) Koka, K.; Besio, W. G. Improvement of spatial selectivity and decrease of mutual information of tri-polar concentric ring electrodes. *J. Neurosci. Methods* **2007**, *165* (2), 216−222.

(60) Zhang, Y.; He, P.; Luo, M.; Xu, X.; Dai, G.; Yang, J. Highly stretchable polymer/silver nanowires composite sensor for human health monitoring. *Nano Res.* **2020**, *13*, 919−926.

(61) Zahed, M. A.; Das, P. S.; Maharjan, P.; Barman, S. C.; Sharifuzzaman, M.; Yoon, S. H.; Park, J. Y. Flexible and robust dry electrodes based on electroconductive polymer spray-coated 3D porous graphene for long-term electrocardiogram signal monitoring system. *Carbon* **2020**, *165*, 26−36.

(62) Shahandashti, P. F.; Pourkheyrollah, H.; Jahanshahi, A.; Ghafoorifard, H. Highly conformable stretchable dry electrodes based on inexpensive flex substrate for long-term biopotential (EMG/ECG) monitoring. *Sens. Actuators, A* **2019**, *295*, 678−686.

(63) Lo, L.-W.; Zhao, J.; Aono, K.; Li, W.; Wen, Z.; Pizzella, S.; Wang, Y.; Chakrabartty, S.; Wang, C. Stretchable sponge electrodes for long-term and motion-artifact-tolerant recording of high-quality electrophysiologic signals. *ACS Nano* **2022**, *16* (8), 11792−11801.

(64) Besio, W.; Aakula, R.; Koka, K.; Dai, W. Development of a tri-polar concentric ring electrode for acquiring accurate Laplacian body surface potentials. *Ann. Biomed. Eng.* **2006**, *34*, 426−435.

https://doi.org/10.1021/acsami.4c04357
ACS Appl. Mater. Interfaces 2024, 16, 27952−27960